

ORIGINAL ARTICLE

Space cooling using geothermal single-effect water/lithium bromide absorption chiller

Mamdouh El Haj Assad¹  | Milad Sadeghzadeh²  | Mohammad Hossein Ahmadi³  |
Mohammad Al-Shabi⁴  | Mona Albawab¹ | Amjad Anvari-Moghaddam⁵ |
Ehab Bani Hani⁶

¹Sustainable and Renewable Energy Engineering Department, University of Sharjah, Sharjah, UAE

²Department of Renewable Energy and Environmental Engineering, University of Tehran, Tehran, Iran

³Faculty of Mechanical Engineering, Shahrood University of Technology, Shahrood, Iran

⁴Mechanical Engineering Department, University of Sharjah, Sharjah, UAE

⁵Department of Energy, Aalborg University, Aalborg, Denmark

⁶School of Engineering, Mechanical Engineering Department, Australian College of Kuwait, Mishref, Kuwait

Correspondence

Mohammad Hossein Ahmadi, Faculty of Mechanical Engineering, Shahrood University of Technology, Shahrood, Iran.
Email: mohammadhosein.ahmadi@gmail.com

Abstract

This research is proposed to fully investigate the performance of a single-effect water/lithium bromide absorption chiller driven by geothermal energy. Since absorption cycles are considered as low-grade energy cycles, this innovative idea of rejecting fluid from a single-flash geothermal power plant with low-grade energy would serve as efficient, economical, and promising technology. In order to examine the feasibility of this approach, a residential building which is located in Sharjah, UAE, considered to evaluate its cooling capacity of 39 kW which is calculated using MATLAB software. Based on the obtained cooling load, modeling of the required water/lithium bromide single-effect absorption chiller machine is implemented and discussed. A detailed performance analysis of the proposed model under different conditions is performed using Engineering Equation Solver software (EES). Based on the obtained results, the major factors in the design of the proposed system are the size of the heat exchangers and the input heat source temperature. The results are presented graphically to find out the geofluid temperature and mass flow and solution heat exchanger effectiveness effects on the chiller thermal performance. Moreover, the effects of the size of all components of the absorption chiller on the cooling load to meet the space heating are presented. The thermal efficiency of the single-flash geothermal power plant is about 13% when the power plant is at production well temperature 250°C, separator pressure 0.24 MPa, and condenser pressure 7.5 kPa. The results show that the coefficient of performance (COP) reaches about 0.87 at solution heat exchanger effectiveness of 0.9, when the geofluid temperature is 120°C.

KEYWORDS

absorption chiller, geothermal power plant, lithium bromide, space cooling

This is an open access article under the terms of the Creative Commons Attribution License, which permits use, distribution and reproduction in any medium, provided the original work is properly cited.

© 2021 The Authors. *Energy Science & Engineering* published by Society of Chemical Industry and John Wiley & Sons Ltd.

1 | INTRODUCTION

Energy-water consumption is a critical topic in the field of energy and environment.¹⁻⁵ Due to fossil fuels being in such a limited amount and the continuous use of coal and natural gas for electricity generation, which result in harmful emissions for community, the use of a clean source of energy is of utmost importance.⁶⁻⁸ Geothermal energy is the thermal energy stored underground due to the earth's core. It radiates from the earth's core; then, the heat is transferred by convection and conduction through different layers of the earth, and it is available in many different forms and in different proportions throughout the world.⁹ Utilization of the geothermal energy is an alternative sustainable and renewable source of power with almost no greenhouse gas emissions and no noise; therefore, no pollution is generated in its surrounding environment.^{10,11} The operation cost is low, and no cost of fuel is needed in case of electricity generation.¹² Geothermal energy handholds a high potential as it is a dependable source of power generation that can operate base load of electricity needs continuously throughout the day and night.^{13,14} Besides, it is very efficient and effective in direct use for heating, cooling, distillation, and other industrial applications.¹⁵⁻¹⁸

There are many fields in which geothermal energy can be applied. This vast field of precious energy can be indirectly exploited for power generation by using the geofluid in liquid phase which is changed later into steam to drive a steam turbine for electricity production¹⁹⁻²¹ or can directly be used for heating and cooling purposes, whether by passing it directly through pipes to radiators to heat a specific place, or by using absorption chillers which take advantage of the geothermal heat to cool a space by a refrigeration cycle.^{22,23} There are many other direct application of geothermal energy, especially for industrial use, such as food drying, distillation, and desalination.^{24,25} Many different factors can affect the method of using geothermal energy, like the cost, quality, and lifetime of the geothermal energy source.²⁶⁻²⁸

Geothermal energy can be used to generate electricity using different types of geothermal power plants which are single-flash steam, double-flash steam, dry-steam power plants, and binary cycle power plants.²⁹⁻³¹ The most common geothermal power plant is the single-flash steam power plant, which is considered as the first power plant that installed using a liquid dominated geothermal field.

Single-flash power covers about 29% of all geothermal plants, and it has around 43% of total installed geothermal power capacity.^{32,33} The power capacity ranges for single-flash power plant from three MW to 117 MW with an average power of about 27 MW.³⁴ In order to run a single-flash power plant of 30 MW, five to six geothermal production wells are needed with at least two to three reinjection wells. Due to the high pressure of a geothermal well, the well of single-flash power plant is in liquid phase.³⁵ This type of geothermal

power plants is best suited to be connected to a single absorption chiller, where the latter runs on waste low-grade thermal energy.³⁶ Therefore, the reinjected geothermal fluid which is colder than the initial geofluid is perfect to provide energy for a single absorption chiller.

Many studies were conducted on absorption chillers due to their dependency on the available low-grade energy.³⁷⁻⁴² Such studies showed that absorption chillers powered by the waste heat from existing power plants showed very promising results although the use of geothermal heat in an absorption chiller is not very common nowadays. Wang et al⁴³ suggested a case study by the University of Western Australia to investigate the possibility of applying a geothermal single-effect absorption chiller system at the main campus. The purpose was to cover the base load requirement for air conditioning and to analyze the feasibility of this project and economical cost. At a depth of 2.5-3 km, they extracted hot ground water at a temperature in the range of 90°C to 100°C in order to cover the campus base cooling load of 1 MW to 3 MW. They used a cascaded geothermal-absorption chiller system in order to convert as much of the thermal energy as possible. The ground water (90-100°C) is first used in the single-effect absorption chiller for cooling, and the used ground water that has a lower temperature between 80°C and 85°C was used to drive another single-effect absorption chiller before the reinjection of the geofluid back to the ground. The achieved COP of the cascade chillers system was 0.67, while the COP of the first absorption chiller was 0.74 and the COP of the second chiller was 0.6. They also found that the time period for the project to payback was about 11-13 years. Ketfi et al⁴⁴ made a probability study for the evaluation of low capacity absorption cooling system and the performance at 5 different climate zones in Algeria, which were named as zone areas E1, E2, E3, E4, and E5. The single-effect absorption chiller of 17.6 kW was simulated with a solar energy source. The chiller was capable of producing chilled water of 7°C at five different zones having different climate conditions. For zones E1 and E2 of ambient temperatures between 30 and 40°C, the chiller was successful in supplying chilled water at 7°C with 37% of the capacity. For zones E3 and E4 where the ambient temperatures were above the range of 30-40°C, it was not possible to produce chilled water at 7°C, but when the chilled water temperature was increased to 12°C, the single absorption chiller reached 45% of its nominal capacity for zone E3 and 33% for zone E4. For zone E5, the absorption chiller was not able to operate due to the very high ambient temperature, which was either due to poor efficiency or the crystallization of LiBr. As a proposed solution for the problem in zone E5, a geothermal heat exchanger was proposed, since the soil temperature was lower than ambient and was constant throughout the year; hence, it would be a preferred alternative to use solar thermal heat source for places with hot climates. Salehi et al⁴⁵ studied

and optimized a double-flash geothermal power plant which was integrated with absorption chiller and freshwater production unit. It was concluded that the integration of absorption chiller was performing 17% better than the other layout. Abdullah et al⁴⁶ carried out an experimental study on the application of geothermal-absorption cooling in Sivas, Turkey. Based on the reported results, geothermal energy in Sivas was not practical for power production but would be feasible for refrigeration and would provide considerable economic output. Recently, the application of single-flash geothermal power plants has been the focus of many research works.^{47,48} Moreover, recent studies on obtaining cooling load from double effect water/LiBr absorption chiller powered by geothermal energy connected in series and parallel configurations have been conducted.^{49,50}

The objective of this research is to study the effect of geofluid temperature, solution heat exchanger effectiveness, size of heat exchangers, and mass flow rate on the performance of single-effect lithium bromide—water absorption chiller powered by single-flash geothermal power plant to determine the best possible option for providing cooling load for a house made of two floors, which is located in Sharjah, UAE. This work also presents a novel approach by considering the climate conditions in the analysis and to find out the required cooling capacity of a household under hot and humid climate conditions. According to the authors' knowledge, this is the first work of an absorption chiller power by geothermal energy presented for the Gulf

region. The results of this parametric study will provide HVAC engineers and researchers with a detailed idea about the geo-chiller performance and the parameters effecting this combination, and it will guide them to have a clear picture about the performance of such integrated system in the design phase.

2 | METHODOLOGY

2.1 | Thermodynamic analysis of single-flash steam power plant

The schematic diagram of single-flash steam power plant combined with single-effect absorption chiller is shown in Figure 1. The power plant receives saturated liquid from the production well. The steam is flashed into liquid and vapor when passing through the throttling valve, after which it is directed to an adiabatic separator in order to separate vapor from liquid. The separated steam enters a steam turbine for electricity production, while the liquid is pumped back to the ground through the injection well. Steam that leaves the turbine goes directly to the condenser where it is condensed; then, the produced saturated liquid is pumped and mixed with saturated liquid leaving the adiabatic separator. The resulted liquid mixture which is at a temperature above 100°C is circulated in the generator of the absorption chiller, after which it is reinjected back to the ground.

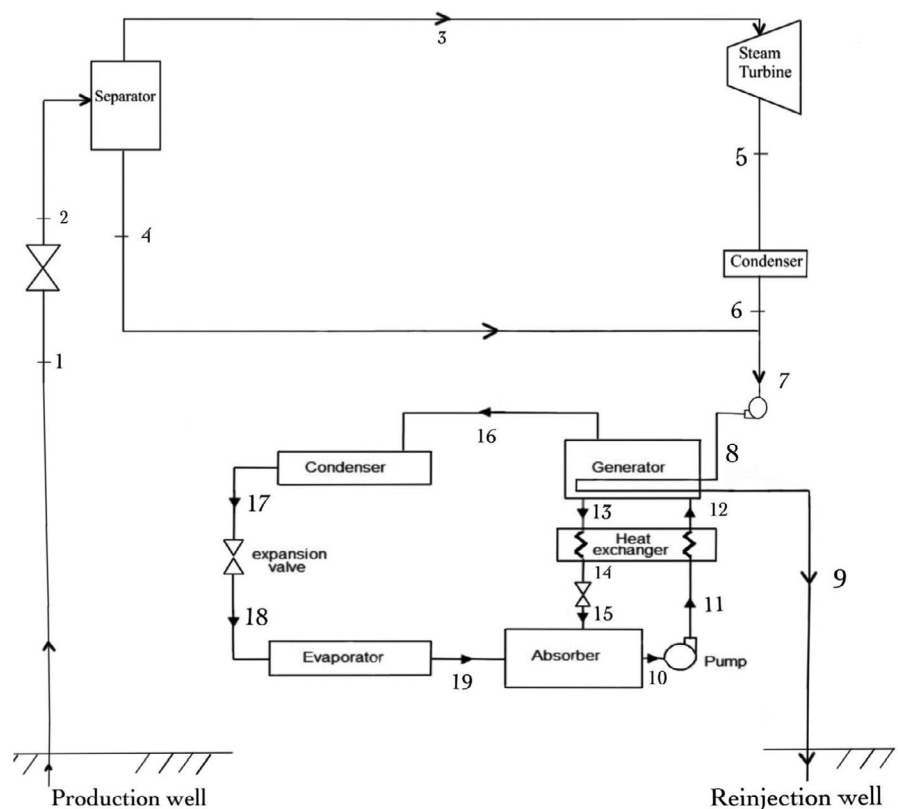


FIGURE 1 Schematic diagram of single-flash steam power plant with absorption chiller

2.1.1 | Mass balance

The mass balance equations are obtained as follows:

$$\dot{m}_1 = \dot{m}_2 = \dot{m}_7 = \dot{m}_8 = \dot{m}_9 \quad (1)$$

$$\dot{m}_4 = (1 - x_2) \dot{m}_2 \quad (2)$$

where x is the vapor quality which is defined as the ratio of the mass flow rates of water vapor and mixture.

$$\dot{m}_3 = \dot{m}_5 = \dot{m}_6 = x_2 \dot{m}_2 \quad (3)$$

2.1.2 | Energy balance

The energy balance equations of each component are written as follows:

Expansion valve:

$$h_1 = h_2 \quad (4)$$

where

$$h_1 = h_f \text{ at } T_1 \quad (5)$$

The steam quality at state 2 can be calculated as

$$x_2 = \frac{h_2 - h_f}{h_{fg}} \quad (6)$$

which is needed to calculate the mass flow rate of saturated vapor and saturated steam leaving the separator.

Separator:

$$\dot{m}_2 h_2 = \dot{m}_3 h_3 + \dot{m}_4 h_4 \quad (7)$$

where

$$h_3 = h_f \text{ at } P_{sep} \quad (8)$$

and

$$h_4 = h_g \text{ at } P_{sep} \quad (10)$$

Steam turbine:

The specific enthalpy of state 6 can be obtained using the following equations:

$$x_{5s} = \frac{s_{5s} - s_f}{s_{fg}} \quad (10)$$

where s is the specific enthalpy and the subscript s refers to the isentropic turbine case.

$$s_{5s} = s_4 = s_g \text{ at } P_{cond} \quad (11)$$

where P_{sep} is the separator pressure. The separator is operating at constant pressure and temperature.

The specific enthalpy at states 5s and 5 is obtained, respectively, as follows:

$$h_{5s} = h_f + x_{5s} h_{fg} \quad (12)$$

$$h_5 = h_4 - \eta_T (h_4 - h_{5s}) \quad (13)$$

where η_T is the isentropic efficiency of the steam turbine.

Condenser:

The exit specific enthalpy at state 7 is obtained from writing the energy balance as follows:

$$\dot{m}_4 h_4 = \dot{m}_6 h_6 + \dot{m}_7 h_7 \quad (14)$$

where $h_6 = h_f$ at P_{cond}

Pump:

The pump work is obtained using the following equations:

$$h_{8s} - h_7 = v_7 (P_8 - P_7) \quad (15)$$

where v is the specific volume.

The isentropic efficiency of the pumps is expressed as

$$\eta_P = \frac{h_{8s} - h_7}{h_8 - h_7} \quad (16)$$

The input parameters for this power plant are the geofluid mass flow rate, geofluid temperature, separator pressure, and condenser pressure. Then by the help of these parameters, the enthalpy of the geofluid entering the desorber (generator) of Figure 1 can be obtained. Knowing this enthalpy, then the temperature can be obtained from water steam tables for the saturated liquid state.

2.2 | Absorption chiller operating principles

Single-effect absorption chiller consists of a generator (desorber), absorber, condenser, evaporator, expansion valve, pump, and solution heat exchanger. Lithium bromide solution as absorbent is flowing in the solution heat exchanger, generator, and absorber, while water as refrigerant is circulating in the condenser and the evaporator.

The lithium bromide solution leaving the absorber has low concentration of lithium bromide and the solution leaving the generator has high concentration of lithium bromide. The weak solution is pumped to the generator where heat is added by the geothermal fluid to evaporate water from the lithium bromide solution. The evaporator vapor goes to the condenser, and the rich solution of lithium bromide is sent

back to the absorber after it passes through the solution heat exchanger and throttling valve to have low pressure prior to absorber entrance.⁵¹ Since the generator and condenser are operating at the same high pressure, a pump is needed to increase the solution pressure after leaving the absorber. Moreover, the absorber and the evaporator are operating at the same low pressure; hence, throttling valves are needed to cause a pressure drop in the absorbent and the refrigerant. Solution heat exchanger is an effective device in absorption chiller because the solution heading to the absorber releases heat to the solution going to the generator, which results in better generator thermal performance in producing vapor.

In most common absorption chillers, there are two main working fluids which are lithium bromide/water and ammonia/water. Water/ lithium bromide is the commonly used working fluids in absorption chillers for space cooling because the operating temperature of such chillers is above 0°C. Many reasons lead to choosing lithium bromide solution namely the good enthalpy of vaporization of water, stability, and relatively high latent heat. Furthermore, lithium bromide is free of toxins and is not harmful to the environment. In addition to that, experimentally the pair of lithium bromide/water has higher COP. Although due to the freezing temperature of water at 0°C, the absorption chiller with lithium bromide/water solution cannot be used for cooling at temperature lower than 4°C to avoid freezing in the pipes of the chiller. Hence, absorption chillers using lithium bromide are recommended for air conditioning.

For steady state processes in the absorption chiller, the mass and energy balance equations of absorption chiller components are shown in Table 1.

The coefficient of performance of the absorption chiller is defined as follows:

$$\text{COP} = \frac{\dot{Q}_e}{\dot{Q}_g} \quad (17)$$

TABLE 1 Balance equations of mass and energy

| System components | Mass balance equation | Energy balance equation |
|-----------------------------|--|--|
| Solution pump | $\dot{m}_1 = \dot{m}_2$ | $\dot{W}_{\text{pump}} = \dot{m}_2 h_2 - \dot{m}_1 h_1$ Neglecting pump work $h_2 = h_1$ |
| Solution expansion valve | $\dot{m}_5 = \dot{m}_6$ | $\dot{m}_5 h_5 = \dot{m}_6 h_6$ $h_5 = h_6$ |
| Solution heat exchanger | $\dot{m}_2 = \dot{m}_3$ $\dot{m}_4 = \dot{m}_5$ | $\dot{m}_2 h_2 + \dot{m}_4 h_4 = \dot{m}_3 h_3 = \dot{m}_5 h_5$ |
| Generator | $\dot{m}_3 = \dot{m}_4 + \dot{m}_7$ | $\dot{Q}_g = \dot{m}_4 h_4 + \dot{m}_7 h_7 - \dot{m}_3 h_3$ |
| Refrigerant expansion valve | $\dot{m}_8 = \dot{m}_9$ | $\dot{m}_8 h_8 = \dot{m}_9 h_9$ |
| Condenser | $\dot{m}_7 = \dot{m}_8$ | $\dot{Q}_c = \dot{m}_7 h_7 - \dot{m}_8 h_8$ |
| Evaporator | $\dot{m}_9 = \dot{m}_{10}$ | $\dot{Q}_e = \dot{m}_{10} h_{10} - \dot{m}_9 h_9$ |
| Absorber | $\dot{m}_1 = \dot{m}_6 + \dot{m}_{10}$ | $\dot{Q}_a = \dot{m}_6 h_6 + \dot{m}_{10} h_{10} - \dot{m}_1 h_1$ |

where \dot{Q}_e and \dot{Q}_g are the heat transfer rates of the evaporator and generator, respectively.

The solution heat exchanger effectiveness is obtained as

$$\epsilon_{SHE} = \frac{T_{13} - T_{14}}{T_{13} - T_{11}} \quad (18)$$

The heat transfer rate of the generator, absorber, condenser, and evaporator is expressed in the following general form.

$$\dot{Q} = UA\Delta T_{lm} \quad (19)$$

where UA is the overall heat transfer coefficient and ΔT_{lm} is the log mean temperature difference.

The absorption chiller in this study is operating between high and low pressures of 7.406 kPa and 0.676 kPa, respectively, and between high and low lithium bromide concentrations of 62.16% and 56.48%, respectively. Sample calculations for the absorption chiller, which include the enthalpy, mass flow rate, and temperature are presented in Table 2 for the operating pressures and lithium bromide concentration at heat source temperature (generator inlet temperature or temperature leaving the geothermal power plant) of 100°C. Table 3 shows the values of heat rates of generator, absorber, condenser, evaporator, solution heat exchanger and pump work, log mean temperature difference, and COP of the absorption chiller.

2.3 | Space cooling load calculation

In this section, a summary of the method used to calculate the cooling load of a chosen residential building in Sharjah, UAE, as shown in Figure 2. The building has two floors and consists of four bedrooms, six bathrooms, two living rooms,

TABLE 2 Thermodynamic properties of state points

| State points | h (kJ/kg) | \dot{m} (kg/s) | P (kPa) | x (vapor quality) | T (°C) | X_{LiBr} (kg/kg) | Remarks |
|--------------|-------------|------------------|-----------|---------------------|----------|--------------------|--|
| 8 | 419.1 | 1 | 300 | 0 | 100 | 0 | Compressed liquid water |
| 9 | 404.3 | 1 | 300 | 0 | 96.51 | 0 | Compressed liquid water |
| 10 | 87.76 | 0.05 | 0.676 | 0 | 32.72 | 0.5648 | Saturated solution, low pressure |
| 11 | 87.77 | 0.05 | 7.406 | 0 | 32.72 | 0.5648 | Subcooled liquid solution, high pressure |
| 12 | 149.9 | 0.05 | 7.406 | 0 | 63.61 | 0.5648 | Subcooled liquid solution, high pressure |
| 13 | 223.3 | 0.04543 | 7.406 | 0 | 89.36 | 0.6216 | Saturated liquid solution, high pressure |
| 14 | 155.0 | 0.04543 | 7.406 | 0 | 53.11 | 0.6216 | Subcooled liquid solution, high pressure |
| 15 | 155.0 | 0.04543 | 0.676 | 0.005 | 44.96 | 0.6216 | Vapor-liquid solution, low pressure |
| 16 | 2643.1 | 0.00457 | 7.406 | - | 76.76 | 0 | Superheated water vapor, high pressure |
| 17 | 167.8 | 0.00457 | 7.406 | 0 | 40.06 | 0 | Saturated liquid water, high pressure |
| 18 | 167.8 | 0.00457 | 0.676 | 0.065 | 1.39 | 0 | Saturated water mixture, low pressure |
| 19 | 2503.1 | 0.00457 | 0.676 | 1 | 1.39 | 0 | Saturated water vapor, low pressure |

TABLE 3 The performance of components and overall system

| Element | \dot{Q} (kW) |
|-------------------------|----------------|
| Generator | 14.7 |
| Evaporator | 10.7 |
| Condenser | 11.3 |
| Absorber | 14.1 |
| Solution heat exchanger | 3.1 |
| Solution pump power | 0.02 |
| COP = 0.73 | |

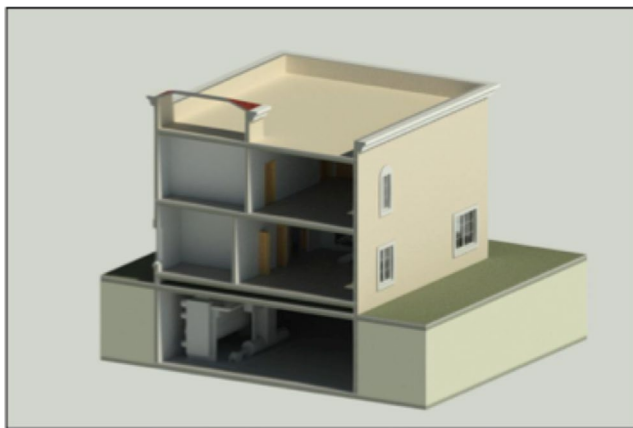


FIGURE 2 3D model of the residential house

one store, one maid room, and a kitchen, with a total area of 312 m², out of which an occupied area of 183 m² needs to be cooled.

The cooling load was calculated using the standard specifications of the American Society of Heating, Refrigerating

and Air-Conditioning Engineers (ASHRAE). The methodology followed using these standards presents the cooling load of a specified space as the amount of heat required to be removed from the area and which is transferred to that space by conduction through the building walls, roof, floor, doors, and by radiation through fenestration and infiltration such as windows and skylights as well as the heat gained by the electric lights, equipment, occupancies, and other activities which take place in that area. Extracting this heat from the space will make the air reach the required design temperature and relative humidity, which meet the standard comfort zone of this method.

The following design parameters given in Table 4 were used as input parameters for calculating the cooling load using ASHRAE standards.

To calculate the cooling load using the mentioned methodology, each part of the chosen building was treated as a separate space from the whole building. In other words, the heat gained in each part via its windows, doors, lights, occupancies, and activities was calculated separately; then, the total heat gained in all the parts was summed up to get the total cooling load required for the entire building.

The calculations must be carried out for each single hour during the day, which means that the process must be repeated 24 times if it is required to calculate the cooling load of one day in the year. In the present study, the calculations were done for ten active hours during one day in the month of August. To calculate the maximum cooling load required for the entire building, the peak of each graph which is called the rush hour which represents the maximum heat gain of each part of the building. By summing up all these peaks, the total heat gain in the building will represent the required cooling load. The heat gain in all spaces of the building is shown in Figure 3. For example, Figure 3G shows that the maximum heat gain in the kitchen is about 4.5 kW; hence, this

TABLE 4 Cooling load design conditions for Sharjah, UAE

| Parameter | Values | Units |
|--|--------|---------------------|
| Indoor conditions | | |
| Indoor temperature, T_i | 24 | °C |
| Indoor relative humidity | 50 | % |
| Outdoor conditions | | |
| Dry bulb temperature, $T_{db,o}$ | 40 | °C |
| Wet bulb temperature, $T_{wb,o}$ | 28 | °C |
| Maximum temperature, $T_{max,o}$ | 43 | °C |
| Mean temperature, $T_{m,o}$ | 35 | °C |
| Adjacent space temperature, T_{adj} | 29 | °C |
| Cooling degree days | 17 | °C |
| Latitude | 25.35 | °N |
| Longitude | 55.42 | °E |
| Overall heat transfer coefficient of walls | | |
| U_W | 1.2 | W/m ² °C |
| U_C | 1.8 | W/m ² °C |
| U_F | 2.1 | W/m ² °C |
| U_G | 6.7 | W/m ² °C |
| U_D | 3.5 | W/m ² °C |

amount of cooling load is required for the kitchen. Similarly, the maximum the heat gains in the rest of the house spaces shown in Figure 3A-I are summarized in Table 5 from which it is found that the total heat gain by the whole space is about 39 kW, which is the amount of cooling load that is required to be provided by the absorption chiller. Figure 3G shows that the heat demand increases to reach a maximum value at around 16 PM after which it decreases as the day is close to sunset time.

3 | RESULTS AND DISCUSSION

3.1 | Parametric study of geothermal single water/LiBr absorption chiller

A parametric study is provided in this section in order to evaluate the behavior of geothermal single absorption chiller and how the mass flow rate of the geofluid, generator inlet temperature, effectiveness of the solution heat exchanger, and size of heat exchangers affect the performance of the absorption chiller. In order to determine the chiller performance, information about the parameters of geothermal power plant is needed, which are production well temperature of 250°C, separator pressure of 0.24 MPa, and condenser pressure of 7.5 kPa. At these input values, the thermal efficiency of the single-flash geothermal power plant is about 12.9%.

3.1.1 | Effect of the desorber inlet temperature, T_8

One of the key components in the design of the absorption chiller is the inlet temperature of the heat source that provides heat to the generator. In this paper, it is considered that the thermal source for the chiller is the hot fluid leaving the geothermal power plant prior to its entrance to the reinjection well. To operate a single-effect water/lithium bromide absorption chiller, the supplied heat needs to be at least at 90°C. This condition is well achieved by the proposed heat source in this work. The temperature of the heat source is a strong parameter which influences all other parameters in the cycle. Figure 4 shows the behavior of the cycle represented by its cooling COP and cooling capacity versus the heat source inlet temperature at different solution heat exchanger effectiveness and at heat source mass flow rate of 1 kg/s. In all the graphs presented in Figure 4, the following behavior can be noticed:

The cooling capacity of the evaporator is increasing, while the COP is decreasing as the supplied geofluid heat temperature is increasing. This can be explained by the fact that increasing the temperature of the geofluid in the desorber results in higher heat supply to the desorber. Moreover, the rate at which the heat supply in the desorber increases is higher than the rate of the cooling rate increase in the evaporator, which leads to a decrease in COP according to Equation (17). Increasing the effectiveness of the solution heat exchanger results in better absorption chiller performance as from the COP trend shown in Figure 4, which is slightly higher than the trend given at the same geofluid inlet temperature of the generator.

Figure 5 shows the effect of solution heat exchanger effectiveness on the COP as the geofluid inlet temperature changes. The figure shows that increasing the geofluid inlet temperature always results in a decrease in COP for all values of solution heat exchanger effectiveness. Moreover, Figure 5 shows that the cooling load increases as the geofluid inlet temperature increases for all solution heat exchanger effectiveness values.

Figures 6 and 7 show the same comparison and behavior of the COP and the cooling capacity but at different heat source inlet mass flow rates of 10 kg/s and 50 kg/s, respectively. The same discussion can be repeated here for Figure 8 but with observing that the machine behavior at different heat source mass flow rates is strongly tied with the size of the internal solution heat exchanger which represented by its effectiveness. No changes in the machine performance with the change in the heat source mass flow rate as long as the size of this heat exchanger does not change.

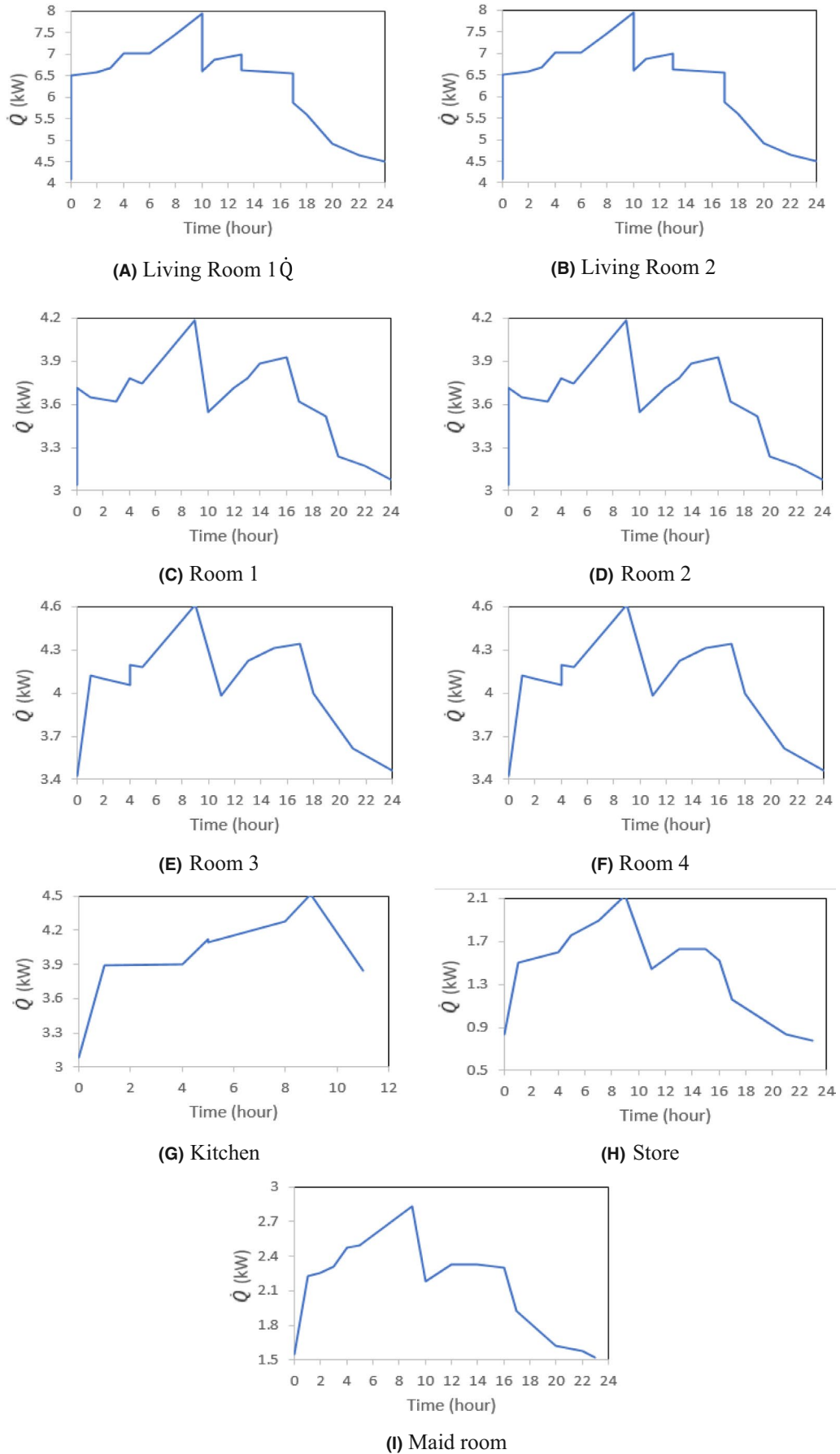


FIGURE 3 Heat gain in each space of the building

TABLE 5 Required cooling load

| Occupied hall | Area (m ²) | Heat gain (kW) |
|-----------------------------|------------------------|----------------|
| Living room 1 | 35.1 | 6.92 |
| Living room 2 | 24.75 | 5.94 |
| Room 1 (master mood) | 22.5 | 4.158 |
| Room 2 (master mood) | 22.5 | 4.16 |
| Room 3 (master mood) | 22.5 | 4.6 |
| Room 4 (master mood) | 22.5 | 4.6 |
| Maid room (master mood) | 6.75 | 2.83 |
| Kitchen | 23.5 | 4.5 |
| Store | 3 | 2.15 |
| Total required cooling load | | 39 kW |

change in the mass flow rate of the geofluid. Figure 9 shows the results at geofluid temperature $T_8 = 90^\circ\text{C}$, which is the case with the mass flow rates of all the heat exchangers of the chiller. This can be explained in a way that the increase in mass flow rate results in smaller exit temperature and hence the increase in the mass flow rate compensates for the decrease in the exit temperature of the heat exchanger, which results in almost unchanged cooling load and COP.

3.1.3 | Effect of solution heat exchanger effectiveness ε

The solution heat exchanger is a key component in the design of any absorption chiller. This is because of its strategic ef-

FIGURE 4 Effect of T_8 on COP and cooling capacity at (A) $\varepsilon_{SHE} = 0.6$ and (B) $\varepsilon_{SHE} = 0.65$ ($\dot{m}_8 = 1 \text{ kg/s}$)

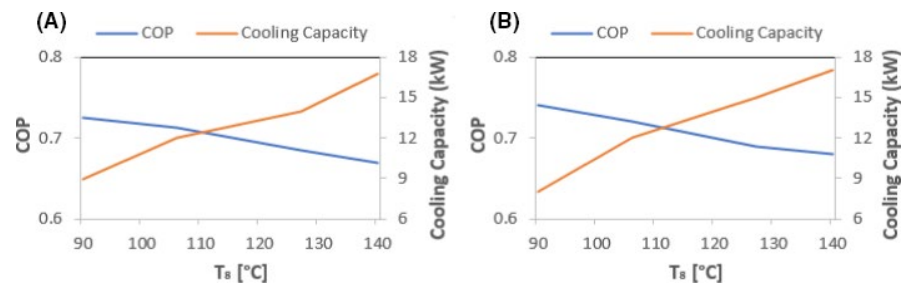


FIGURE 5 Effect of T_8 on (A) COP and (B) cooling capacity for different effectiveness values ($\dot{m}_8 = 1 \text{ kg/s}$)

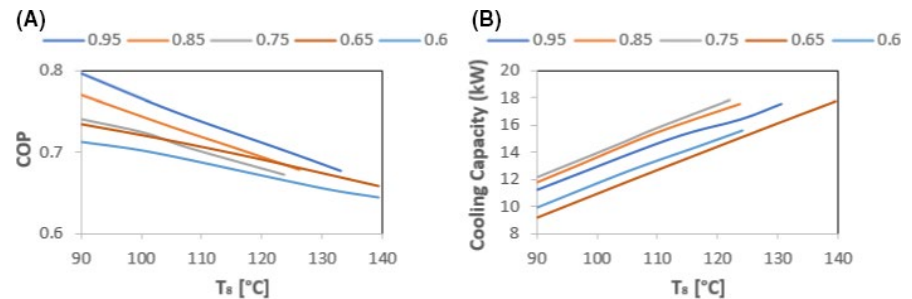
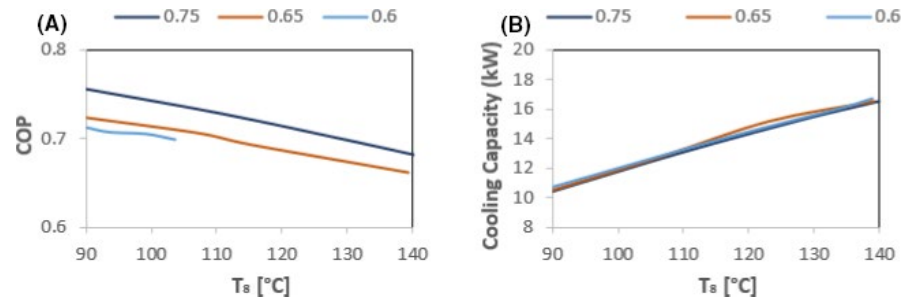


FIGURE 6 Effect of T_8 on (A) COP and (B) cooling capacity for different effectiveness values ($\dot{m}_8 = 10 \text{ kg/s}$)



3.1.2 | Effect of the heat source inlet mass flow rate

In Figure 9A,B, it can be seen that the COP and the cooling capacity of the chiller show very little sensitivity to the

effective location in the configuration of the chiller which lies as a connecting point between the high-pressure side of the machine represented by the generator, and the low-pressure side represented by the absorber. Therefore, any change in this component will result in changing the heat transfer

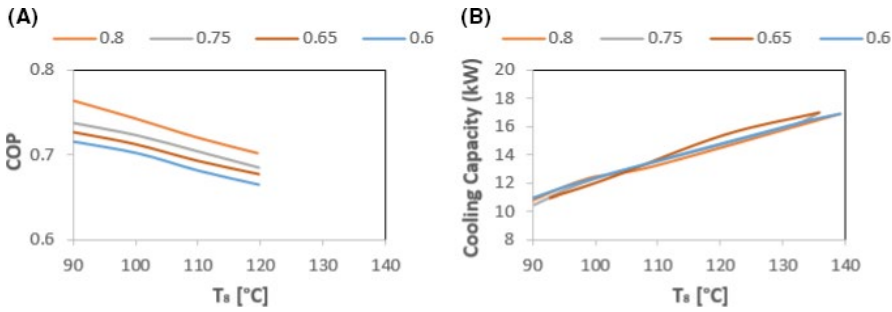


FIGURE 7 Effect of T_8 on (A) COP and (B) cooling capacity for different effectiveness values ($\dot{m}_8 = 50$ kg/s)

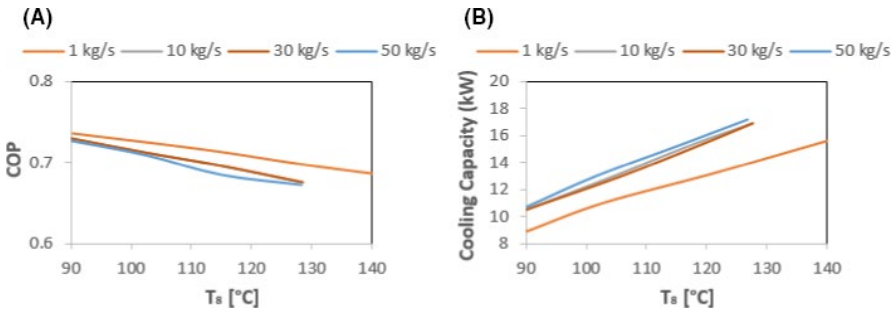


FIGURE 8 Effect of T_8 on (A) COP and (B) cooling capacity for different values of \dot{m}_8 ($\epsilon = 0.65$)

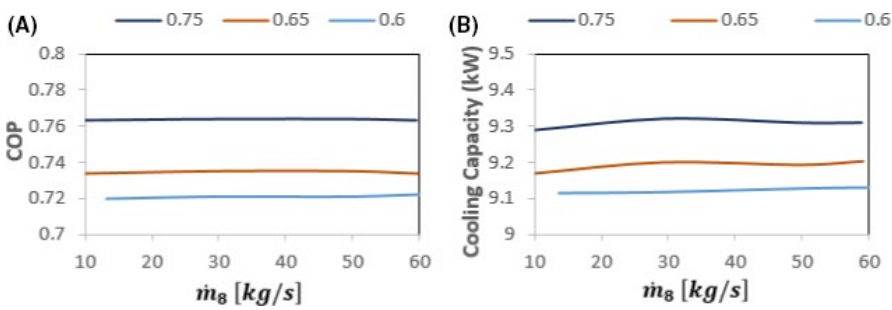


FIGURE 9 Effect of \dot{m}_8 on (A) COP and (B) cooling capacity for different values of ϵ ($T_8 = 90^\circ\text{C}$)

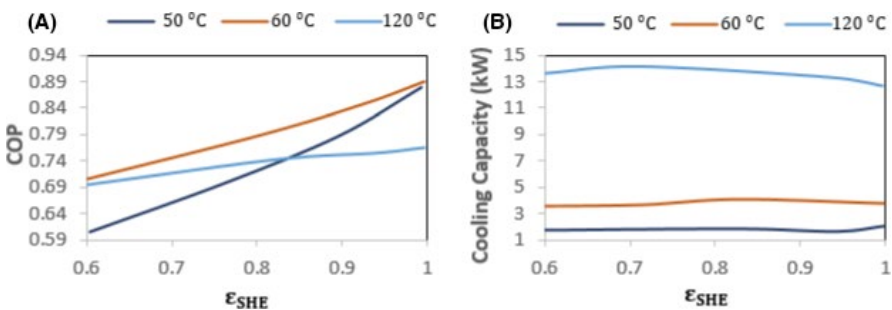


FIGURE 10 Effect of ϵ on (A) COP and (B) cooling capacity for different values of T_8 ($\dot{m}_8 = 10$ kg/s)

requirements in both the generator and the absorber, and thus the COP. Figure 10 shows how the COP is strongly influenced by the solution heat exchanger effectiveness. This is due to the high influence on the generator operating conditions because it is directly affected by the performance of the solution heat exchanger. This is true for all the geofluid inlet temperature to the desorber. Figure 10 also shows the effect of ϵ_{SHE} on the cooling capacity of the chiller. The trends of performance at different geofluid inlet temperatures show that the cooling capacity is slightly increasing with the increase in the effectiveness for geofluid inlet temperature to

the desorber between 70 and 100°C. Hence, it can be stated the effectiveness of the solution heat exchanger has more direct influence on the heat transfer load of the desorber and absorber rather than the evaporator.

3.1.4 | Effect of heat exchangers sizes

Another design parameter that has been examined is the size of the implemented heat exchangers in the absorption chiller. The sizes are represented by the UA values of the heat

exchangers. This effect is shown in Figure 11. In all cases, it is observed the same trend of the COP and the cooling capacity of the chiller against the size of all the heat exchangers at different heat source input temperatures. In all cases, the cooling capacity is increasing exponentially with the size of the heat exchangers due to the increase in the area of the heat exchanger. The COP is increasing significantly as the size of the evaporator increases as shown in Figure 11A. As well as, the increase in the evaporator area results in an increase in the cooling load. The increase in UA means either increase in U and A, or increase in one of them, which results in better heat transfer characteristics of the evaporator, hence resulting in higher COP and cooling load as UA increases. The same results are obtained for the desorber, absorber, and condenser except for the COP variation when considering the changes in the overall heat transfer coefficient of the desorber (Figure 11B). This figure shows that COP increases to a maximum value after which it decreases with increasing the overall heat transfer coefficient. This is due to the fact that increasing UA of the desorber results in higher values of heat input to the desorber at a higher rate than that in the evaporator for UA values above 0.25 as can be seen from Figure 11B, hence from the COP definition, COP decreases as higher values of desorber UA.

The variation of COP with UA_d for different heat source temperature values at heat exchanger effectiveness of 0.64 is shown in Figure 11B. Figure 11B shows that increasing the overall heat transfer coefficient of the desorber results in an increase in the COP. This is due to the fact that the amount of water vapor generated in the desorber increases with increasing the heat source temperature; in other words, the mass flow of the refrigerant increases which in turns results in increasing the cooling load of the evaporator. Figure 11B

also shows that increasing the heat source temperature results in an increase in the cooling load for the same heat exchanger effectiveness. The figure shows that for heat source of 90°C , the cooling load cannot be computed at large values of UA_d due to the possible LiBr crystallization problem. Figure 11C shows the variation of COP with the absorber overall heat transfer coefficient for different heat source temperature values at $\varepsilon = 0.64$. The figure shows that COP is monotonically increasing with UA_a . This increase in UA_a results in improving the heat transfer characteristics of the absorber to absorb more water vapor coming from the evaporator as can be seen from Figure 11C which shows an increase in the cooling load due to the increase in the refrigerant (water) mass flow rate. Figure 11C shows that it is not recommended to operate the absorption chiller at 90°C and 110°C at UA_a values higher than 1.9 and 2.5, respectively, due to the possible crystallization of LiBr.

Figure 11D shows the variation of COP and cooling load with the overall heat transfer coefficient of the condenser for different heat source temperatures at $\varepsilon = 0.64$, respectively. The figure shows that increasing UA_c results in increasing COP and \dot{Q}_e . The increase in both parameters is sharp up to $UA_c = 1.1$ after which the increase becomes smooth. Increasing the overall heat transfer coefficient of the condenser will improve the heat transfer characteristics of the condenser which will in turn results in better evaporator performance which results in an increase in the COP.

4 | CONCLUSIONS

In conclusion, this paper aims to analyze the performance of a water/lithium bromide single-effect absorption chiller

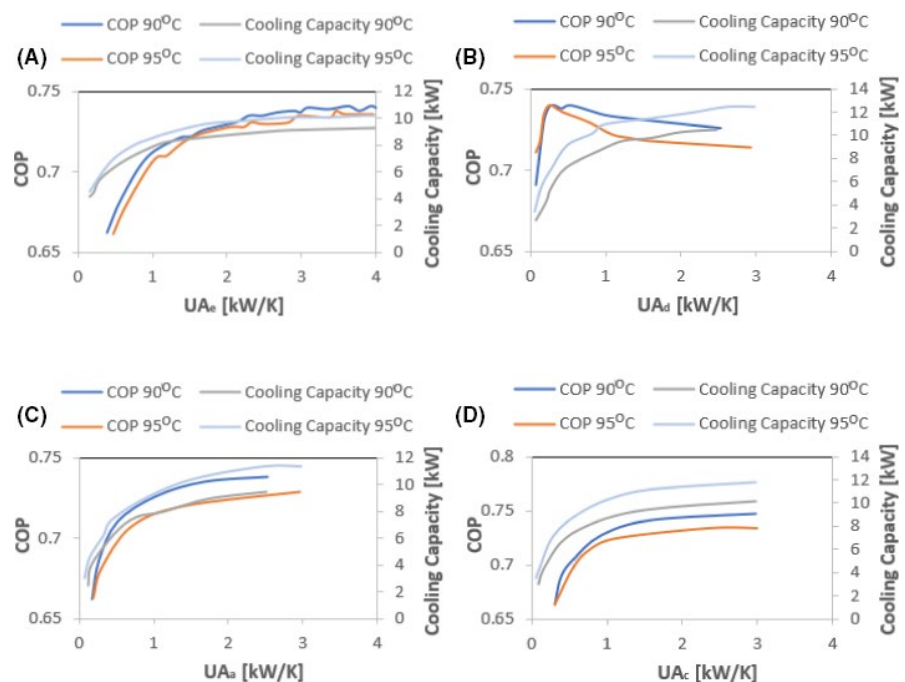


FIGURE 11 COP and cooling capacity for variation in (A) UA_e , (B) UA_d , (C) UA_a , and (D) UA_c for different values of T_8 ($\varepsilon = 0.64$)

driven by geothermal energy drained from a geothermal power plant after consuming part of the enthalpy of the hot fluid for electricity generation. This had been done through a pure research approach by proposing a model and performing a parametric study on the proposed model. The partial analysis that was done showed that the proposed absorption machine is a really promising technology in replacing the conventional air conditioning devices due to many reasons. As a main reason that it can operate with an accepted COP using a low-grade energy such as the heat carried by the geothermal fluid prior to its reinjection back to the earth through the rejection well. Thus, the cooling load obtained by using the waste heat from existing geothermal power plants is free of cost. Moreover, these machines have the advantage of low or even no noise while operating which is considered as disadvantage in conventional air conditioning. The parametric study showed that the input heat source temperature and the sizes of the heat exchangers are the key components in the design of absorption chiller. The thermal efficiency of the geothermal power plant is 12.9% and the COP is 0.87 when the plant is running at 250°C, 0.24 MPa, and 7.5 kPa as geothermal well temperature, separator pressure, and condenser pressure, respectively.

More analysis approaches would be done in the future by examining wider range of operating conditions to further investigate the full picture about the performance of these machines.

Nomenclature

| | |
|-----------|--|
| A | area (m ²) |
| COP | coefficient of performance |
| h | enthalpy (kJ/kg) |
| \dot{m} | mass flow rate (kg/s) |
| p | pressure (Pa) |
| \dot{Q} | heat transfer rate (kW) |
| T | temperature (°C) |
| U | heat transfer coefficient (W/m ² K) |
| X | lithium bromide concentration |

Greek letters

| | |
|------------------|---------------------------------------|
| ϵ_{SHE} | solution heat exchanger effectiveness |
| ΔT_{lm} | log mean temperature difference (K) |

Subscripts

| | |
|-------|----------------------|
| a | absorber |
| ADJ | adjacent space |
| c | condenser |
| C | ceiling |
| d | desorber (generator) |
| D | door |
| db | dry bulb |
| e | evaporator |
| F | floor |

| | |
|-----|----------------------|
| g | generator (desorber) |
| G | ground |
| i | inside |
| m | outside mean |

CONFLICT OF INTEREST

The authors declare that they do not have any conflicts of interest.

ORCID

Mamdouh El Haj Assad  <https://orcid.org/0000-0001-6311-7925>

Milad Sadeghzadeh  <https://orcid.org/0000-0001-8574-5463>

Mohammad Hossein Ahmadi  <https://orcid.org/0000-0002-0097-2534>

Mohammad Al-Shabi  <https://orcid.org/0000-0002-9540-3675>

REFERENCES

- Qin Y, He Y, Hiller JE, Mei G. A new water-retaining paver block for reducing runoff and cooling pavement. *J Clean Prod.* 2018;199:948-956.
- Qin Y. A review on the development of cool pavements to mitigate urban heat island effect. *Renew Sustain Energy Rev.* 2015;52:445-459.
- Qin Y, Zhang M, Hiller JE. Theoretical and experimental studies on the daily accumulative heat gain from cool roofs. *Energy.* 2017;129:138-147.
- Qin Y, He Y, Wu B, Ma S, Zhang X. Regulating top albedo and bottom emissivity of concrete roof tiles for reducing building heat gains. *Energy Build.* 2017;156:218-224.
- Qin Y. Pavement surface maximum temperature increases linearly with solar absorption and reciprocal thermal inertial. *Int J Heat Mass Transf.* 2016;97:391-399.
- Mehrpooya M, Sadeghzadeh M, Rahimi A, Pouriman M. Technical performance analysis of a combined cooling heating and power (CCHP) system based on solid oxide fuel cell (SOFC) technology – a building application. *Energy Convers Manag.* 2019;198:111767.
- Parisi ML, Ferrara N, Torsello L, Basosi R. Life cycle assessment of atmospheric emission profiles of the Italian geothermal power plants. *J Clean Prod.* 2019;234:881-894.
- Baci AB, Salmi M, Menni Y, Ghafourian S, Sadeghzadeh M, Ghalandari M. A new configuration of vertically connecting solar cells: solar tree. *Int J Photoenergy.* 2020;2020:1-8.
- Zare V, Palideh V. Employing thermoelectric generator for power generation enhancement in a Kalina cycle driven by low-grade geothermal energy. *Appl Therm Eng.* 2018;130:418-428.
- Ghazvini M, Sadeghzadeh M, Ahmadi MH, Moosavi S, Pourfayaz F. Geothermal energy use in hydrogen production: a review. *Int J Energy Res.* 2019;43:7823-7851.
- Kaushal M. Geothermal cooling/heating using ground heat exchanger for various experimental and analytical studies: comprehensive review. *Energy Build.* 2017;139:634-652.
- Siddiqui O, Ishaq H, Dincer I. A novel solar and geothermal-based trigeneration system for electricity generation, hydrogen production and cooling. *Energy Convers Manag.* 2019;198:111812.

13. Kanoğlu M, Çengel YA. Economic evaluation of geothermal power generation, heating, and cooling. *Energy*. 1999;24:501-509.
14. Parikhani T, Ghaebi H, Rostamzadeh H. A novel geothermal combined cooling and power cycle based on the absorption power cycle: energy, exergy and exergoeconomic analysis. *Energy*. 2018;153:265-277.
15. Yu Y, Li H, Niu F, Yu D. Investigation of a coupled geothermal cooling system with earth tube and solar chimney. *Appl Energy*. 2014;114:209-217.
16. Angrisani G, Diglio G, Sasso M, Calise F, Dentice DM. Design of a novel geothermal heating and cooling system: energy and economic analysis. *Energy Convers Manag*. 2016;108:144-159.
17. Ahmadi MH, Banihashem SA, Ghazvini M, Sadeghzadeh M. Thermo-economic and exergy assessment and optimization of performance of a hydrogen production system by using geothermal energy. *Energy Environ*. 2018;29:1373-1392.
18. Mirzaee M, Zare R, Sadeghzadeh M, Maddah H. Thermodynamic analyses of different scenarios in a CCHP system with micro turbine – absorption chiller, and heat exchanger. *Energy Convers Manag*. 2019;198:111919.
19. Seyam S, Dincer I, Agelin-Chaab M. Analysis of a clean hydrogen liquefaction plant integrated with a geothermal system. *J Clean Prod*. 2020;243:118562.
20. Li K, Liu C, Jiang S, Chen Y. Review on hybrid geothermal and solar power systems. *J Clean Prod*. 2020;250:119481.
21. Bonyadi N, Johnson E, Baker D. Technoeconomic and exergy analysis of a solar geothermal hybrid electric power plant using a novel combined cycle. *Energy Convers Manag*. 2018;156:542-554.
22. Kairouani L, Nehdi E. Cooling performance and energy saving of a compression-absorption refrigeration system assisted by geothermal energy. *Appl Therm Eng*. 2006;26:288-294.
23. Behnam P, Arefi A, Shafii MB. Exergetic and thermoeconomic analysis of a trigeneration system producing electricity, hot water, and fresh water driven by low-temperature geothermal sources. *Energy Convers Manag*. 2018;157:266-276.
24. Mertoglu O, Bakir N, Kaya T. Geothermal applications in Turkey. *Geothermics*. 2003;32:419-428.
25. Lund JW, Boyd TL. Direct utilization of geothermal energy 2015 worldwide review. *Geothermics*. 2016;60:66-93.
26. Hepbasli A, Akdemir O. Energy and exergy analysis of a ground source (geothermal) heat pump system. *Energy Convers Manag*. 2004;45:737-753.
27. Hepbasli A, Canakci C. Geothermal district heating applications in Turkey: a case study of Izmir-Balcova. *Energy Convers Manag*. 2003;44:1285-1301.
28. Keçebaş A. Energetic, exergetic, economic and environmental evaluations of geothermal district heating systems: an application. *Energy Convers Manag*. 2013;65:546-556.
29. Bravi M, Basosi R. Environmental impact of electricity from selected geothermal power plants in Italy. *J Clean Prod*. 2014;66:301-308.
30. Hienuki S, Kudoh Y, Hondo H. Life cycle employment effect of geothermal power generation using an extended input-output model: the case of Japan. *J Clean Prod*. 2015;93:203-212.
31. Coskun C, Oktay Z, Dincer I. Thermodynamic analyses and case studies of geothermal based multi-generation systems. *J Clean Prod*. 2012;32:71-80.
32. Pambudi N, Itoi R, Jalilinasrabad S, Jaelani K. *Performance Improvement of Single-Flash Geothermal Power Plant Applying Three Cases Development Scenarios Using Thermodynamic Methods*; 2015.
33. El Haj AM, Bani-Hani E, Khalil M. Performance of geothermal power plants (single, dual, and binary) to compensate for LHC-CERN power consumption: comparative study. *Geotherm Energy*. 2017;5:17.
34. Pambudi NA, Itoi R, Jalilinasrabad S, Jaelani K. Performance improvement of a single-flash geothermal power plant in Dieng, Indonesia, upon conversion to a double-flash system using thermodynamic analysis. *Renew Energy*. 2015;80:424-431.
35. D'Amore F, Celati R. Methodology for calculating steam quality in geothermal reservoirs. *Geothermics*. 1983;12:129-140.
36. Han B-C, Cheng W-L, Nian Y-L, Yang L, Zhao R. Evaluation of an ammonia-water absorption long-distance cooling/heating system for enhanced geothermal resources. *Energy Convers Manag*. 2019;192:346-358.
37. Qin X, Chen L, Xia S. Ecological performance of four-temperature-level absorption heat transformer with heat resistance, heat leakage and internal irreversibility. *Int J Heat Mass Transf*. 2017;114:252-257.
38. Qin X, Chen L, Ge Y, Sun F. Thermodynamic modeling and performance analysis of the variable-temperature heat reservoir absorption heat pump cycle. *Phys A Stat Mech Appl*. 2015;436:788-797.
39. Qin X, Chen L, Ge Y, Sun F. Finite time thermodynamic studies on absorption thermodynamic cycles: a state-of-the-art review. *Arab J Sci Eng*. 2013;38:405-419.
40. Qin X, Lingen C, Fengrui S. Thermodynamic modeling and performance of variable-temperature heat reservoir absorption refrigeration cycle. *Int J Exergy*. 2010;7:521-534.
41. Chen L, Zheng T, Sun F, Wu C. Irreversible four-temperature-level absorption refrigerator. *Sol Energy*. 2006;80:347-360.
42. Qin X, Chen L, Sun F, Wu C. Thermo-economic optimization of an endoreversible four-heat-reservoir absorption-refrigerator. *Appl Energy*. 2005;81:420-433.
43. Wang X, Bierwirth A, Christ A, Whittaker P, Regenauer-Lieb K, Chua HT. Application of geothermal absorption air-conditioning system: a case study. *Appl Therm Eng*. 2013;50:71-80.
44. Ketfi O, Merzouk M, Merzouk NK, Bourouis M. Feasibility study and performance evaluation of low capacity water-LiBr absorption cooling systems functioning in different Algerian climate zones. *Int J Refrig*. 2017;82:36-50.
45. Salehi S, Mahmoudi SMS, Yari M, Rosen MA. Multi-objective optimization of two double-flash geothermal power plants integrated with absorption heat transformation and water desalination. *J Clean Prod*. 2018;195:796-809.
46. Keçeciler A, Acar Hİ, Doğan A. Thermodynamic analysis of the absorption refrigeration system with geothermal energy: an experimental study. *Energy Convers Manag*. 2000;41:37-48.
47. El Haj AM, Ahmadi MH, Sadeghzadeh M, Yassin A, Issakhov A. Renewable hybrid energy systems using geothermal energy: hybrid solar thermal-geothermal power plant. *Int J Low-Carbon Technol*. 2020;16:518-530.
48. El Haj AM, Aryanfar Y, Radman S, Yousef B, Pakatchian M. Energy and exergy analyses of single flash geothermal power plant at optimum separator temperature. *Int J Low-Carbon Technol*. 2021:ctab014. <https://doi.org/10.1093/ijlct/ctab014>
49. El Haj AM, Khosravi A, Said Z, Albawab M, Salameh T. Thermodynamic analysis of geothermal series flow double-effect water/LiBr absorption chiller. In: *2019 Advances in Science and Engineering Technology International Conferences (ASET)*,

- Dubai, United Arab Emirates; 2019:1-6. <https://doi.org/10.1109/ICASET.2019.8714468>
50. El Haj AM, Said Z, Khosravi A, Salameh T, Albawab M. Parametric study of geothermal parallel flow double-effect water-LiBr absorption chiller. In: *2019 Advances in Science and Engineering Technology International Conferences (ASET)*, Dubai, United Arab Emirates; 2019:1-6. <https://doi.org/10.1109/ICASET.2019.8714434>
51. Yilmaz C. Thermodynamic and economic investigation of geothermal powered absorption cooling system for buildings. *Geothermics*. 2017;70:239-248.

How to cite this article: El Haj Assad M, Sadeghzadeh M, Ahmadi MH, et al. Space cooling using geothermal single-effect water/lithium bromide absorption chiller. *Energy Sci Eng*. 2021;9:1747–1760. <https://doi.org/10.1002/ese3.946>